Lithospheric Mantle Evolution beneath the Eifel (Germany): Constraints from Sr–Nd–Pb Isotopes and Trace Element Abundances in Spinel Peridotite and Pyroxenite Xenoliths

G. WITT-EICKSCHEN[1,2,3]*, H. A. SECK[1], K. MEZGER[3], S. M. EGGINS[4] AND R. ALTHERR[2]

[1]INSTITUT FÜR MINERALOGIE UND GEOCHEMIE DER UNIVERSITÄT KÖLN, ZÜLPICHER STR. 49B, D-50674 COLOGNE, GERMANY

[2]MINERALOGISCHES INSTITUT DER UNIVERSITÄT HEIDELBERG, IM NEUENHEIMER FELD 236, D-69120 HEIDELBERG, GERMANY

[3]INSTITUT FÜR MINERALOGIE DER UNIVERSITÄT MÜNSTER, CORRENSSTR. 24, D-48149 MÜNSTER, GERMANY

[4]RESEARCH SCHOOL OF EARTH SCIENCES, THE AUSTRALIAN NATIONAL UNIVERSITY, CANBERRA, A.C.T. 0200, AUSTRALIA

The Pb isotope compositions of amphiboles and clinopyroxenes in spinel peridotite and pyroxenite mantle xenoliths from the intra-plate Quaternary volcanic fields of the Eifel province (Germany) are strongly correlated with their Sr–Nd isotope and trace element compositions. High-temperature anhydrous xenoliths from a depth of around 60 km have trace element and Sr–Nd–Pb isotope compositions similar to the depleted source of mid-ocean ridge basalts (Depleted MORB Mantle, DMM). Amphibole-bearing xenoliths from shallower depths (<45 km) provide evidence for three temporally distinct episodes of mantle metasomatism in the subcontinental lithosphere: (1) aqueous fluids from an isotopically enriched (EM-like) mantle reservoir caused amphibole formation during deformation in the shallow continental lithospheric mantle and may be subduction related, probably associated with the last major tectonic event that influenced the area (Hercynian orogeny). (2) During a second phase of mantle metasomatism the EM-like lithospheric mantle was affected by melts from an ancient, HIMU-like (high time-integrated $\mu = {}^{238}U/{}^{204}Pb$) mantle source. The HIMU-like component introduced by these fluids had a much more radiogenic Pb isotope composition than the asthenospheric source of the widespread Cenozoic magmatism in Europe and may be linked to reactivation of ancient subducted crustal domains during the Hercynian orogeny or to early Cretaceous deep-sourced mantle plumes. (3) During a brief final stage the heterogeneously enriched EM–HIMU subcontinental lithosphere was locally modified by basaltic melts migrating along fractures and veins through the upper mantle as a consequence of the Cenozoic Eifel volcanism. Although a DMM component is completely lacking in the metasomatic fluids of the metasomatic episodes 1 and 2, the vein melts of episode 3 and the Cenozoic Eifel lavas require mantle sources containing three end-member components (DMM–HIMU–EM). Thus, mobilization of the more depleted mantle material occurred at the earliest in the Tertiary, contemporaneously with the development of the extensive rift system and main melt generation in Europe. Alternatively, the variety of Sr–Nd–Pb isotope signatures of the metasomatic agents may have been produced by melting of isotopically distinct mantle domains in a heterogeneous uprising mantle plume.

KEY WORDS: *Eifel; Europe; mantle xenoliths; metasomatism; Pb isotopes*

*Corresponding author. Present address: Institut für Mineralogie und Geochemie der Universität Köln, Zülpicher Str. 49B, D-50674 Cologne, Germany. Telephone: ++49 221 470 3170. Fax: ++49 221 470 5199. E-mail: Gudrun.Witt-Eickschen@uni-koeln.de

INTRODUCTION

The Cenozoic western and central European volcanic provinces are spatially and temporally linked to the development of an extensive intra-continental rift system and domal uplift of Hercynian basements in connection with the collision of the African and Eurasian plates (Wilson & Downes, 1991; Wilson & Patterson, 2001). The most primitive mafic rocks within these volcanic fields share many of the Sr–Nd–Pb isotope and geochemical characteristics of plume-related ocean island basalts (OIB) (e.g. Wedepohl & Baumann, 1999). Thus, the chemical composition of the lavas appears to be consistent with an origin from a mantle plume, but seismic or geological evidence for partial melting in a large ascending mantle plume is lacking. Instead, seismic tomographic studies indicate the presence of small, finger-like bodies of low-velocity material extending from ~70 km to at least 400 km in the upper mantle beneath these areas (Granet et al., 1995; Ritter et al., 2001; Keyser et al., 2002). Whereas previous studies emphasized the difficulty in reconciling partial melting in such small mantle diapirs with plume dynamics (Wilson & Downes, 1991; Wedepohl et al., 1994; Hegner et al., 1995), more recent models recognize this as a distinct type of mantle convection (e.g. Wilson & Patterson, 2001). Cenozoic magma generation is associated with these small-scale zones of diapiric upwelling and thus the source of the OIB-like component is inferred to be located at the base of the upper mantle or even in the lower mantle (Wedepohl & Baumann, 1999; Wilson & Patterson, 2001).

Although the abundant spinel peridotite mantle xenoliths exhumed from the subcontinental lithosphere beneath Europe by the Cenozoic magmas do not necessarily provide information about the source region of the most primitive basalts, they might provide a component within the lithospheric mantle that contributed to the isotope and geochemical characteristics of asthenosphere-derived magmas. These mantle xenoliths show a much wider range in Nd–Sr isotope compositions than their Cenozoic host basalts and provide important constraints on the nature and geochemical evolution of the lithospheric upper mantle beneath Europe (e.g. Downes, 2001). This raises the following questions: (1) Is the variable metasomatic enrichment of the subcontinental lithosphere related to the Cenozoic intra-plate magmatism of Europe or is it the fingerprint of much earlier metasomatic events? (2) Are the metasomatic agents plume or asthenosphere derived, or released from recycled ancient mafic subducted crust? (3) Did a lithospheric mantle, similar to that represented by

the xenoliths, play a role in the petrogenesis of the Cenozoic lavas?

To address these questions we present a study of Pb isotope compositions in conjunction with new trace element data for different types of lithospheric mantle xenoliths (Table 1) from the Quaternary volcanic fields of the Eifel (Germany), for which, with the exception of some samples, Nd–Sr isotopic data have already been published (Stosch et al.,

Table 1: Mineral modes and equilibrium temperatures (T) for peridotites and magmatic veins selected for Pb isotopic analysis

	ol	cpx	opx	sp	amph	phlog	T (°C)*
LREE-depleted, anhydrous high-temperature xenoliths							
DWD58	0·69	0·09	0·22	0·01			1185
DWK1	0·69	0·10	0·20	0·01			1240
Modally metasomatized, equigranular recrystallized xenoliths							
MM262	0·66	0·05	0·23	0·01	0·05		1023
MM278	0·62	0·08	0·24	0·02	0·03		968
MM766	0·60	0·02	0·33	0·02	0·02		1027
DW194	0·85	0·01	0·11	0·02	0·02		1028
DW211	0·80	0·04	0·11	0·03	0·03		955
DW284	0·63	0·06	0·26	0·03	0·01		902
DW582	0·68	0·06	0·22	0·01	0·03		949
Modally metasomatized, porphyroclastic xenoliths							
EE157	0·67	0·06	0·22	0·03	0·03		763
EE158	0·70	0·05	0·18	0·02	0·05		756
EE159	0·70	0·06	0·21	0·03	0·02		872
Pyroxenite veins							
DW327	0·25	0·75					1171
DW328	0·12	0·88					1183
DW906	0·24	0·76					1119
DW918	0·24	0·76					1132
Peridotitic wall rock adjacent to pyroxenite vein							
DW328	0·75	0·04	0·21	0·01			1183
Hornblendite veins							
MM214	0·05				0·65	0·30	
MM262					0·88	0·12	1023
MM313					0·93	0·07	1072
MM326					0·98	0·02	1004
Peridotitic wall rocks adjacent to hornblendite veins							
MM271	0·79	0·07	0·10	0·01	0·02		1081
MM214	orthopyroxene-free wehrlite with amphibole and phlogopite						

*Temperatures are calculated using the two-pyroxene thermometer of Brey & Köhler (1990) for a pressure of 1·5 GPa; temperatures for the porphyroclastic xenoliths were calculated from the pyroxene neoblast compositions; for magmatic veins the temperatures of the peridotitic host rocks are given.

1980; Stosch & Lugmair, 1986; Witt-Eickschen & Kramm, 1998*b*; Witt-Eickschen *et al.*, 1998). Supplementing these data with Pb isotopes has the distinct advantage that the mantle components are much better constrained than by Nd–Sr isotope correlations alone. Based on the extreme Sr–Nd–Pb isotope compositions of young oceanic basalts, Zindler & Hart (1986) distinguished four end-member components in the Earth's mantle: DMM (depleted upper mantle representing the source of mid-ocean ridge basalts), EM1 and EM2 (enriched mantle), and HIMU (high time-integrated $\mu = {}^{238}U/{}^{204}Pb$; widely considered to reflect ancient recycled oceanic crust). These reservoirs and isotope signatures are thought to be produced by the formation and recycling of oceanic crust and lithosphere, plus small amounts of recycled continental crust. Wörner *et al.* (1986) proposed an additional end-member composition for continental basalts (PREMA = prevalent mantle), which is isotopically enriched relative to DMM and interpreted as the reactivated 'fossilized' heads of mantle plumes that were unable to penetrate the continental lithosphere (Stein & Hofmann, 1992). Depleted DMM-like components present in plumes seem to differ from the present-day DMM source by having a higher Hf isotope ratio (e.g. Iceland lavas, Kempton *et al.*, 2000) and are probably generated by ancient melting events. Moreover, most hotspots have distinct isotopic 'flavours' (Hofmann, 1997) that are not necessarily related to mixing of melts or material from the isotopically distinct end-member components but may be due to melting of mantle domains with specific isotopic and geochemical characteristics.

The Sr–Nd–Pb isotope compositions of the mantle xenoliths are used to constrain the geochemical characteristics and source of the metasomatic agents that enriched the shallow subcontinental lithospheric mantle beneath the Eifel. In addition, we have studied pyroxenite and hornblendite veins occurring in composite mantle xenoliths that crystallized from parental melts generated from sub-lithospheric mantle sources. As the vein melts are clearly unmodified by crustal effects and genetically related to the Cenozoic alkali basalts from the Eifel (Witt-Eickschen & Kramm, 1998*b*; Witt-Eickschen *et al.*, 1998), they retain the original isotopic characteristics of the mantle source of the intra-plate lavas.

ANALYTICAL PROCEDURES

Incompatible trace element abundances in amphiboles and clinopyroxenes were measured *in situ* by laser ablation inductively coupled plasma mass spectrometry (LA-ICP-MS) at the Research School of Earth Sciences (ANU) in Canberra. Ablation was performed in a He atmosphere using an ArF EXIMER laser (193 nm) at 100 mJ/pulse and a 5 Hz pulse repetition rate using an ablation time of 60 s. The ablated material was flushed in a continuous argon flow into the torch of an Agilent 7500 Series ICP-MS system. The silicate glass reference material NIST 612 was analysed and background count rates were measured before and after 10 unknowns for calibration purposes and instrumental drift corrections. To correct for differences in the ablation yield between standard and samples, ${}^{43}Ca$ was used as an internal standard, based on electron microprobe measurements of CaO in the minerals. Replicate routine analyses ($n = 307$) of trace element abundances in basalt glass standard USGS BCR-2G are compared with the data of Norman *et al.* (1998) in Table 2. These analyses yielded the following standard deviations (2σ) of the average concentrations: rare earth elements (REE) (La to Yb) 4–6%, Lu 8%; large ion lithophile elements (LILE) 3–6%; Y 4%, high field strength elements (HFSE) 3–6%; Pb, U and Th 6%; W 16%; Mo 4%. The trace element concentrations reported in Tables 2 and 3 were collected from the grain cores with an 84 μm laser spot size and are averages of 3–9 analyses performed for each mineral. Multiple analyses of grain cores and rims with a 29 μm spot demonstrated that the trace element abundances are homogeneous within individual amphibole and clinopyroxene grains. Further information about analytical details including correction procedures, limits of detection, and instrumental errors has been given by Eggins *et al.* (1998).

Sr–Nd–Pb isotopic analyses of inclusion-free amphiboles, clinopyroxenes, and phlogopites separated by handpicking under a binocular microscope (50–200 mg) were carried out at the Zentrallabor für Geochronologie der Universität Münster. The Sr–Nd isotope data were obtained using the same etching, separation, and analytical methods, including measurement conditions and correction procedures for mass fractionation, given in detail by Witt-Eickschen & Kramm (1998*a*). Repeat analyses yielded an ${}^{87}Sr/{}^{86}Sr$ ratio of $0\cdot71024 \pm 0\cdot00002$ ($n = 55$) for the NBS-987 standard and a ${}^{143}Nd/{}^{144}Nd$ ratio of $0\cdot51184 \pm 0\cdot00002$ ($n = 24$) for the La Jolla Standard. For the Pb isotope analysis amphibole and clinopyroxene separates were leached for 2 h in hot (80°C) 2N HCl and washed in ultra-pure water, whereas phlogopite was decomposed without pretreatment. A ${}^{205}Pb$ spike was added before dissolution of the minerals in HF–HNO$_3$ (5:1). The Pb fraction of the samples was separated by a wash and elution procedure on AG1-X8 anion exchange Teflon columns using 1N HBr and 6N HCl. The sample solution was evaporated down for loading after addition of a drop of 0·25N HNO$_3$. Pb was measured on a single Re filament using the silica

*Table 2: Examples of major and trace element analyses of amphiboles from peridotites and magmatic veins, and trace element data of basalt glass USGS BCR2g (*n = 307*) of this study [TS] and from Norman et al. (1998) [N98]*

	Equigranular recrystallized				Porphyroclastic				Magmatic veins				Wall rock	[TS]	[N98]
	MM262	MM278	MM766	DW211	EE157	EE158	EE159	EE163	MM248	MM251	MM326	MM333	MM271	BCR2g	BCR2g
wt %															
SiO_2	44·14	43·75	44·28	44·49	46·67	45·09	46·22	47·71	44·53	43·93	40·89	41·10	44·24		
TiO_2	0·24	0·27	0·52	0·36	0·26	0·28	0·15	0·15	2·90	1·75	3·67	3·65	0·94		
Al_2O_3	14·59	15·03	14·68	13·35	12·51	12·54	12·59	11·00	12·01	13·00	13·78	13·75	12·80		
Cr_2O_3	1·81	1·43	1·93	2·03	0·87	1·29	1·25	0·93	0·36	0·75	0·01	0·08	2·51		
FeO	4·03	4·15	3·73	4·06	3·68	3·75	4·03	3·54	3·72	4·39	9·59	8·46	4·00		
MnO	0·02	0·04	0·01	0·00	0·02	0·06	0·00	0·04	0·00	0·01	0·06	0·13	0·01		
NiO	0·11	0·12	0·12	0·12	0·13	0·11	0·10	0·10	0·10	0·01	0·02	0·06	0·09		
MgO	17·79	17·74	17·92	18·24	19·41	18·55	18·66	19·43	17·98	18·14	13·78	14·05	18·03		
CaO	10·83	11·26	11·20	10·64	11·93	11·73	11·95	11·60	10·96	11·18	10·81	11·62	10·32		
Na_2O	3·06	3·06	3·08	3·28	2·57	2·82	2·49	2·36	3·39	2·93	2·80	2·62	3·59		
K_2O	1·08	1·10	1·21	0·91	0·23	0·40	0·44	0·46	1·22	1·36	1·75	2·05	1·01		
Total	97·70	97·95	98·68	97·48	98·28	96·62	97·88	97·32	97·17	97·45	97·16	97·57	97·54		
ppm															
Ti	1466	1804	2773	1776	1584	1547	575	821	20562	9925	24875	25378	5003	13714	13700
Rb	21·9	24·4	17·1	7·8	4·0	2·3	2·7	2·9	10·3	15·3	24·0	29·0	8·3	54	49
Sr	568	473	637	905	471	393	77	305	512	605	419	439	607	336	342
Y	14·8	15·7	14·0	20·2	16·8	11·4	5·0	8·8	14·9	22·9	12·3	12·9	16·7	35	35
Zr	22·1	19·3	25·1	41·7	2·1	56	3·4	0·9	182	500	163	103	86	183	194
Nb	100	89	179	144	4·5	0·63	6·1	2·3	49	231	47	35	170	13·1	12·8
Mo	n.a.	0·77	n.a.	0·24	1·23	0·79	0·54	0·89	n.a.	n.a.	n.a.	n.a.	0·21	292	244
Ba	452	648	379	257	316	139	57	121	182	230	337	389	151	681	660
La	36·2	38·4	30·4	45·8	23·9	7·1	6·5	14·3	17·9	41·3	11·5	9·1	26·3	24·5	24·5
Ce	91·4	68·6	84·0	117	25·4	13·1	8·5	14·7	47·0	84·8	33·1	27·4	77·9	52·3	50·5
Nd	38·7	18·4	29·4	61·1	5·0	7·6	1·96	1·82	26·7	36·6	21·7	20·3	42·6	27·6	29·0
Sm	5·5	2·4	3·9	10·5	0·54	1·72	0·36	0·19	5·6	7·6	4·8	4·9	7·0	6·4	6·6
Eu	1·40	0·73	1·07	3·0	0·26	0·50	0·14	0·10	1·83	2·17	1·56	1·54	2·00	1·92	1·92
Gd	3·6	2·0	3·0	7·0	0·93	1·54	0·49	0·48	4·7	6·3	4·1	4·1	4·9	6·4	6·5
Dy	2·6	2·4	2·5	4·2	2·1	1·65	0·71	1·13	3·3	4·8	2·8	3·0	3·2	6·0	6·5
Ho	0·51	0·52	0·50	0·71	0·58	0·40	0·17	0·30	0·57	0·85	0·48	0·47	0·58	1·21	1·31
Er	1·43	1·54	1·40	1·81	2·0	1·31	0·59	1·03	1·36	2·14	1·15	1·16	1·50	3·4	3·6
Yb	1·28	1·45	1·21	1·45	2·2	1·58	0·76	1·17	1·04	1·80	0·86	0·79	1·24	3·2	3·5
Lu	0·18	0·21	0·17	0·21	0·34	0·25	0·12	0·19	0·14	0·26	0·11	0·11	0·17	0·48	0·51
Hf	0·25	0·26	0·33	0·33	(0·06)	0·84	(0·12)	(0·02)	5·9	14·9	5·0	3·3	1·40	4·6	5·0
Ta	3·3	5·1	6·0	4·6	(0·01)	(0·02)	(0·06)	(0·03)	3·2	14·3	3·1	2·2	9·0	0·78	0·78
W	n.a.	0·05	n.a.	0·04	0·25	0·88	0·10	0·45	n.a.	0·05	n.a.	n.a.	0·06	0·57	0·44
Pb	3·2	5·1	2·4	2·2	2·3	4·8	1·54	3·6	1·60	3·5	0·84	0·56	1·83	11·6	11·5
Th	3·8	4·8	1·13	3·1	0·75	0·94	0·38	1·17	1·00	4·0	0·70	0·35	0·69	5·7	6·1
U	0·61	0·94	0·13	0·65	1·10	1·24	0·35	0·92	0·24	0·65	0·17	0·11	0·17	1·75	1·73

Values in parentheses are below detection limit; n.a., not analysed.

Table 3: Examples of major and trace element compositions of clinopyroxenes from amphibole-bearing peridotites and from anhydrous magmatic pyroxenite veins

	Equigranular recrystallized						Porphyroclastic			Wall rock	Magmatic veins	
	MM262	MM278	MM766	DW211	DW284	DW582	EE157	EE158	EE163	MM271	DW328	DW906
wt %												
SiO_2	53·62	53·18	53·22	54·12	52·96	53·37	54·21	54·42	55·02	53·39	51·87	50·85
TiO_2	0·05	0·06	0·08	0·04	0·05	0·05	0·08	0·05	0·05	0·16	0·50	1·14
Al_2O_3	3·34	3·73	4·34	3·11	3·75	3·42	2·42	2·07	1·55	4·15	6·66	6·46
Cr_2O_3	0·59	0·54	0·78	1·05	0·59	0·77	0·32	0·32	0·31	1·51	0·42	1·00
FeO	3·07	2·62	2·55	2·8	2·51	2·43	2·14	2·23	2·08	3·1	4·78	4·15
MnO	0·08	0·07	0·09	0·06	0·08	0·06	0·06	0·06	0·05	0·10	0·11	0·07
NiO	0·04	0·05	0·05	0·05	0·05	0·06	0·06	0·04	0·02	0·05	0·00	0·02
MgO	17·06	16·96	16·63	16·57	16·59	16·90	16·79	17·59	17·45	16·15	16·32	14·77
CaO	21·05	21·91	20·85	20·98	22·12	21·77	23·91	23·35	23·79	19·4	18·84	20·19
Na_2O	0·95	0·74	1·10	1·15	0·88	0·94	0·25	0·31	0·20	1·63	1·03	1·06
Total	99·85	99·86	99·66	99·93	99·56	99·76	100·24	100·44	100·52	99·64	100·53	99·71
ppm												
Ti	242	342	419	239	260	266	411	309	175	1241	4291	6474
Rb	0·20	0·04	0·01	0·01	0·06	0·00	0·03	0·08	0·06	0·00	0·00	0·00
Sr	317	220	278	566	331	216	39	97	62	305	71	112
Y	9·2	8·3	9·0	13·4	7·3	9·0	3·6	1·67	2·6	16·7	8·4	10·2
Zr	12·9	12·7	12·1	24·8	9·2	14·2	(0·07)	12·7	0·28	41·9	23·0	48·9
Nb	0·72	0·55	1·08	0·85	1·52	1·15	(0·06)	(0·03)	(0·06)	1·73	0·28	0·47
Mo	0·11	0·10	n.a.	n.a.	0·10	n.a.	0·34	0·25	0·19	0·09	n.a.	n.a.
Ba	26·8	4·8	0·32	0·54	9·6	0·21	3·3	0·68	1·45	0·32	0·10	0·16
La	26·1	22·5	18·7	31·2	19·7	13·7	5·4	2·02	4·9	19·6	1·92	4·0
Ce	67·0	45·3	54·7	80·2	62·3	39·9	5·8	3·3	5·1	63·1	6·8	13·7
Nd	26·5	13·9	19·5	41·9	27·1	18·8	0·95	1·57	0·59	38·1	6·5	11·6
Sm	3·7	1·79	2·5	7·2	3·3	3·0	0·11	0·32	0·07	6·8	1·95	3·1
Eu	0·96	0·50	0·71	2·06	0·85	0·83	(0·05)	(0·08)	(0·03)	1·95	0·65	0·98
Gd	2·2	1·37	1·89	4·6	1·73	2·02	0·23	0·25	0·13	4·9	1·96	2·82
Dy	1·64	1·35	1·59	2·8	1·20	1·56	0·48	0·28	0·34	3·2	1·57	2·08
Ho	0·32	0·29	0·31	0·48	0·25	0·30	0·13	0·06	0·09	0·59	0·28	0·36
Er	0·92	0·89	0·90	1·23	0·77	0·84	0·44	0·19	0·32	1·50	0·69	0·87
Yb	0·87	0·90	0·84	1·03	0·78	0·80	0·49	0·25	0·40	1·29	0·51	0·62
Lu	0·13	0·13	0·13	0·15	0·12	0·12	0·07	0·04	0·07	0·18	0·07	0·08
Hf	0·16	0·18	0·16	0·20	0·15	(0·12)	(0·03)	0·20	(0·01)	0·52	0·90	1·71
Ta	0·08	0·11	0·12	0·08	0·20	0·14	(0·00)	(0·00)	(0·00)	0·26	0·04	0·12
W	(0·01)	(0·01)	n.a.	n.a.	(0·03)	n.a.	0·31	0·59	0·19	(0·01)	n.a.	n.a.
Pb	1·42	1·46	0·66	0·85	1·12	0·67	0·48	1·10	1·04	0·44	0·04	0·05
Th	2·3	2·5	0·51	2·03	1·73	1·60	0·20	0·29	0·46	0·77	0·03	0·05
U	0·38	0·60	0·08	0·38	0·34	0·24	0·27	0·34	0·43	0·18	0·01	0·01

Values in parentheses are below detection limit; n.a., not analysed.

Table 4: Sr–Nd–Pb isotope compositions of amphiboles and clinopyroxenes from the various types of mantle xenoliths

Sample no.		$^{206}Pb/^{204}Pb$	$^{207}Pb/^{204}Pb$	$^{208}Pb/^{204}Pb$	ppm Pb	$^{87}Sr/^{86}Sr$	$^{143}Nd/^{144}Nd$	$^{147}Sm/^{144}Nd$	
Anhydrous, LREE-depleted, high-temperature peridotites									
DWD58	cpx	18·540	15·563	38·064	0·041	0·70230	0·513346	0·2302	4
DWK1	cpx	17·346	15·519	37·044	0·029	0·70185	0·513243	0·2356	3
Modally metasomatized, equigranular recrystallized peridotites									
MM262	cpx	19·750	15·684	39·893	0·808	0·70409	0·512511	0·0827	2
MM262	am	19·764	15·683	39·895	2·550	n.a.	n.a.	n.a.	
MM278	cpx	19·523	15·677	39·636	1·228	0·70445	0·512561	0·0823	5
MM766	cpx	19·805	15·664	39·902	0·691	0·70380	0·512601	0·0780	5
MM766	am	19·805	15·669	39·891	1·863	0·70382	0·512597	0·0789	5
DW194	cpx	20·340	15·670	40·284	0·772	0·70340	0·512664	0·1072	1
DW211	cpx	20·334	15·688	40·420	0·779	0·70338	0·512617	0·1019	1
DW284	cpx	20·195	15·690	40·215	0·904	0·70345	0·512616	0·0720	1
DW582	cpx	19·992	15·679	40·087	0·563	0·70357	0·512636	0·0946	1
Modally metasomatized, porphyroclastic peridotites									
EE158	am	19·251	15·659	39·267	3·166	0·70494	0·512482	0·1379	5
Pyroxenite veins									
DW327	cpx	19·338	15·671	39·172	0·092	0·70361	0·512803	0·1650	1
DW328	cpx	19·067	15·525	39·001	0·028	0·70361	0·512827	0·2078	1
DW906	cpx	19·343	15·662	39·174	0·061	0·70373	0·512820	0·1579	1
DW918	cpx	18·945	15·616	38·846	0·083	0·70439	0·512687	0·1632	1
Wall rock adjacent to pyroxenite vein									
DW328	cpx	19·464	15·653	39·376	0·063	0·70378	0·512782	0·1667	1
Hornblendite veins									
MM214	am	19·226	15·623	39·315	0·485	0·70376	0·512770	0·1452	2
MM214	ph	19·122	15·652	39·130	0·563	0·70378	n.a.	n.a.	2
MM262	am	19·247	15·596	39·147	n.a.	0·70373	0·512782	0·1305	1
MM313	am	19·382	15·645	39·393	0·412	0·70376	0·512795	0·1174	5
MM326	am	19·431	15·638	39·367	0·705	n.a.	n.a.	n.a.	
Wall rocks adjacent to hornblendite veins									
MM271	cpx	19·623	15·662	39·654	0·344	0·70379	0·512690	0·1049	2
MM214	ph	18·821	15·632	38·793	0·816	n.a.	n.a.	n.a.	

References for Sr–Nd data: 1, Witt-Eickschen & Kramm (1998*b*); 2, Witt-Eickschen *et al*. (1998); 3, Stosch *et al*. (1980); 4, Stosch & Lugmair (1986); 5, this study.

gel–H_3PO_4 emitter technique. The isotope ratios were measured in static multi-collection mode on a VG Sector 54 mass spectrometer at temperatures ranging from 1350 to 1450°C. Where concentrations of Pb were very low (<8 ng Pb) mass 204 was measured with a Daly detector, performing three Daly–Faraday gain calibrations before and after each sample run. All Pb isotope ratios are corrected for a 0·10% fractionation per a.m.u. based on repeat analyses of NBS 982. Total procedural blanks for Pb did not exceed 30 pg Pb during the period of the analytical work and were allowed for in the correction of the data (blank composition: $^{206}Pb/^{204}Pb = 17.72$, $^{207}Pb/^{204}Pb = 15.52$, $^{208}Pb/^{204}Pb = 37.70$). The data determined exclusively by the Faraday cups have a total error of ±0·1%; those determined by the use of the electron multiplier have a total error of ±0·2%. Repeat analyses ($n = 15$) of the NBS 982 standard yielded $^{206}Pb/^{204}Pb = 36.738 \pm 0.032$, $^{207}Pb/^{204}Pb = 17.153 \pm 0.020$, and $^{208}Pb/^{204}Pb = 36.745 \pm 0.054$.
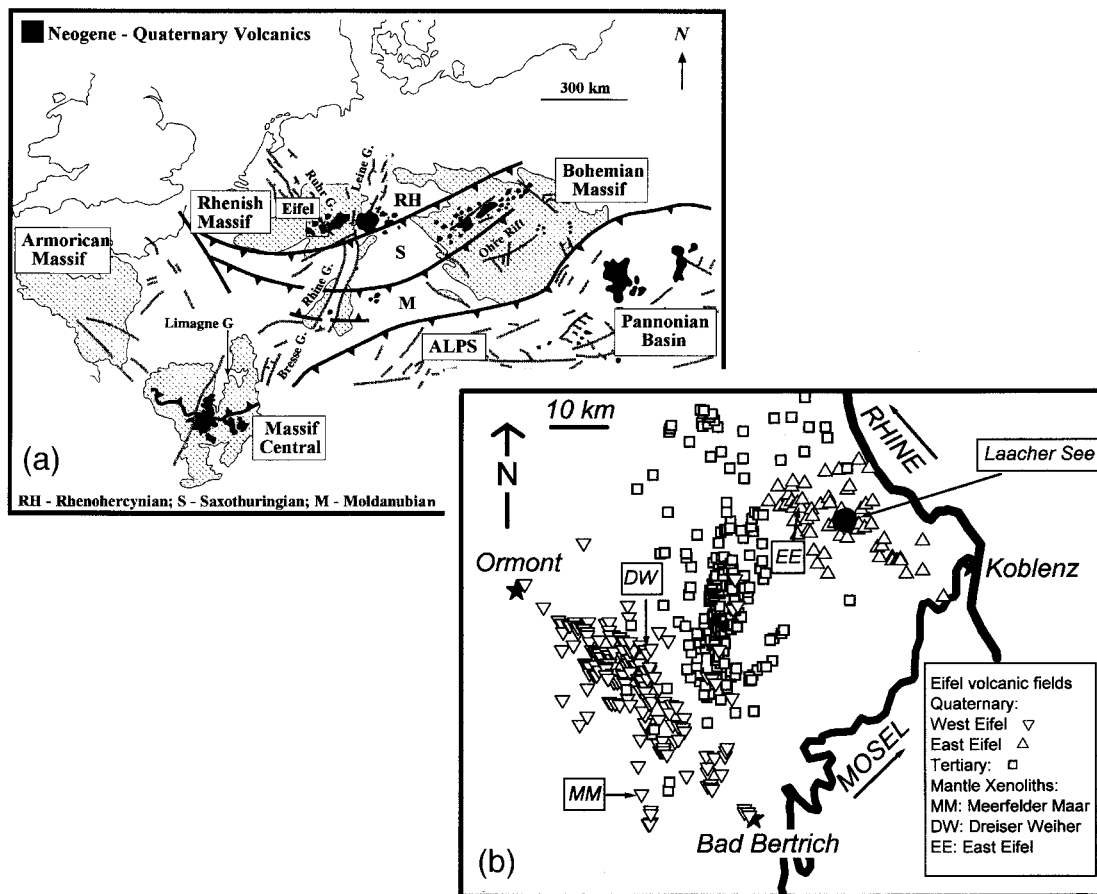
Fig. 1. (a) Map of the western and eastern European volcanic provinces (after Wilson & Downes, 1991). (b) Distribution of the eruptive centres of the Quaternary West and East Eifel (after Mertes & Schmincke, 1985) and of the Tertiary Eifel volcanic fields (after Huckenholz & Büchel, 1988).

PETROGRAPHY OF THE XENOLITHS

The samples analysed in this study include spinel peridotite and pyroxenite xenoliths from basaltic tephra layers of the Quaternary volcanic fields of the West and East Eifel [Fig. 1; West Eifel: Dreiser Weiher (DW), Meerfelder Maar (MM); East Eifel: Olbrück (EE)] that have previously been characterized petrologically and geochemically and for the most part for their Sr–Nd-isotopic composition (Stosch *et al.*, 1980; Stosch & Lugmair, 1986; Stosch, 1987; Witt & Seck, 1989; Witt-Eickschen *et al.*, 1993, 1998; Witt-Eickschen & Harte, 1994; Witt-Eickschen & Kramm, 1998*b*). The modal mineralogy of the samples is listed in Table 1. LA-ICP-MS incompatible trace element abundances and Sr–Nd–Pb isotope data for amphiboles and clinopyroxenes are presented in Tables 2–4. On the basis of their thermal and geochemical characteristics three groups of mantle xenoliths can be identified (Stosch & Seck, 1980; Witt-Eickschen *et al.*, 1993): (1) anhydrous, high-temperature, light REE

(LREE)-depleted peridotites; (2) two types of modally metasomatized xenoliths with texturally equilibrated Ti-poor amphiboles; (3) magmatic clinopyroxenites and hornblendites from vein systems within the lithospheric mantle of the West Eifel.

Anhydrous, high-temperature, LREE-depleted xenoliths

High-temperature (1150–1250°C) coarse-grained (Fig. 2a) to recrystallized spinel peridotites from the West Eifel are anhydrous and were derived from a depth of around 60–65 km (Köhler & Brey, 1990). The lherzolites (Table 1) selected for this investigation lack textural evidence for the existence of a precursor protolith that has equilibrated at even greater depths (e.g. spinel–pyroxene clusters as an indicator of the former presence of garnet).

On the basis of the depletion of LREE in the clinopyroxenes [$(La/Yb)_n = 0.4$–0.6, where subscript n means normalized to the primitive mantle (PM) values of Hofmann (1988)] and their Sr–Nd isotope
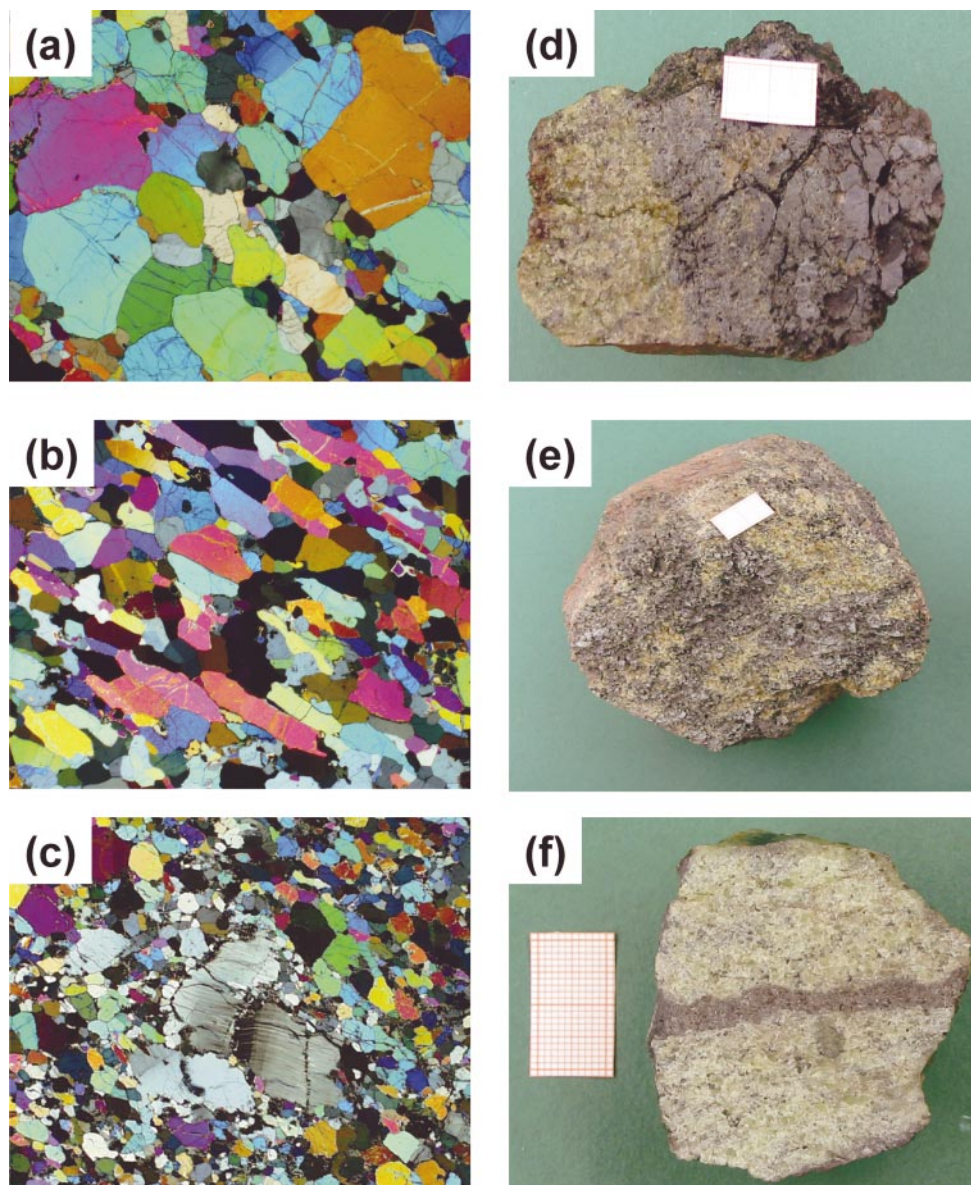
Fig. 2. Representative photomicrographs: (a) the coarse-grained texture; (b) tabular equigranular recrystallized texture; (c) porphyroclastic texture (long side of figures is 1·1 cm). Photographs (scale bar 2 cm) of: (d) a magmatic coarse-grained clinopyroxenite vein (right part) in contact with high-temperature peridotite (left); (e) a discrete olivine-bearing clinopyroxenite xenolith; (f) a hornblendite vein in contact with equigranular recrystallized peridotite.

compositions (Table 4), Stosch *et al.* (1980) suggested that these xenoliths represent fragments of the subcontinental mantle lithosphere with geochemical and isotopic affinities of the mid-ocean ridge basalt source mantle (DMM; Depleted MORB Mantle). Their Sr and Nd model ages were attributed to multistage melting episodes in the sub-Eifel mantle with a main low-degree partial melting event at ∼2 Ga as a result of the formation of continental crust (Stosch, 1987).

Modally metasomatized xenoliths with texturally equilibrated Ti-poor amphiboles

In contrast to the LREE-depleted high-temperature peridotites, the majority of the mantle xenoliths of the West and East Eifel provide strong evidence for metasomatic overprint, which produced compositional and isotopic heterogeneities in the mantle part of the lithosphere. Two texturally distinct types of amphibole-bearing peridotites can be recognized: equigranular recrystallized and porphyroclastic.

Equigranular recrystallized amphibole-bearing xenoliths

Depleted lherzolites to harzburgites (Table 1) with tabular (Fig. 2b) or mosaic equigranular recrystallized textures, which occur in the West Eifel volcanic rocks, are considered to be the products of extensive shearing and recrystallization (e.g. Mercier & Nicolas, 1975). Temperatures of most samples (900–970°C) selected for this study plot within the low-temperature range typical for this xenolith suite (Sachtleben & Seck, 1981). Some xenoliths with chemically zoned orthopyroxene (MM262, MM766, DW194) yield higher temperatures (1020–1030°C) and belong to the group of reheated hydrous peridotites (Witt-Eickschen *et al.*, 1993). CO_2-rich fluid inclusions in the pyroxenes covering a variety of densities and homogenization temperatures suggest an equilibration of the peridotites immediately below the Moho (Witt-Eickschen *et al.*, 2003), which lies at a depth of ∼28 km below the Eifel (Mechie *et al.*, 1983; Raikes & Bonjer, 1983). The xenoliths contain 1–5 wt % tabular pargasite that had attained textural and major and trace element chemical equilibrium with all of the other mineral phases since its formation (Witt & Seck, 1989; Witt-Eickschen & Harte, 1994).

Porphyroclastic amphibole-bearing xenoliths

Deformation during cooling has resulted in the development of porphyroclastic textures in xenoliths from the East Eifel (Witt & Seck, 1989). The xenoliths are characterized by large deformed orthopyroxene porphyroclasts surrounded by a matrix of fine-grained, polygonal-shaped olivine, pyroxene and amphibole neoblasts (Fig. 2c). The equilibration temperatures of an early, high-temperature stage (> 1050°C) have been reconstructed from the bulk composition of the now-exsolved pyroxene porphyroclasts by reintegrating the composition of the host pyroxene with that of the exsolution lamellae (Witt & Seck, 1989; Witt-Eickschen & Harte, 1994). The now-exsolved orthopyroxene porphyroclasts and the clinopyroxene lamellae, as well as the orthopyroxene and clinopyroxene neoblasts, record distinctly lower temperatures (∼800°C) that indicate cooling during recrystallization. The presence of 2–5 wt % pargasite to edenite amphiboles (Table 1) as polygonal neoblasts in the recrystallized matrix and in broken kink bands within the pyroxene porphyroclasts indicates a temporal association between deformation and metasomatic enrichment processes (Witt & Seck, 1989).

Clinopyroxenite and hornblendite magmatic veins and adjacent peridotitic wall rocks

Clinopyroxenite and mica-bearing hornblendite veins of presumed magmatic origin present in composite mantle xenoliths from the West Eifel provide evidence for high-pressure infiltration of silicate melts into the lithospheric mantle (Witt-Eickschen *et al.*, 1993). The effect of these infiltrating melts on the mineralogy, major and trace element and Sr–Nd isotope composition of their peridotitic wall rocks is in most cases limited to distances of several centimetres from the veins (Witt-Eickschen *et al.*, 1993, 1998; Witt-Eickschen & Kramm, 1998*b*). Both clinopyroxenite and hornblendite veins and their peridotitic wall rocks were selected for Pb isotope analysis.

Clinopyroxenite veins

The olivine-bearing clinopyroxenites occur as coarse-grained veins of 1–5 cm width (Fig. 2d) crosscutting anhydrous, high-temperature, peridotite host xenoliths and as discrete xenoliths (Fig. 2e) up to 25 cm in diameter. The vein clinopyroxenes have major element compositions similar to the clinopyroxenes from the non-composite high-temperature lherzolites from the West Eifel, but their Ti contents are distinctly higher (Witt-Eickschen *et al.*, 1993). Witt-Eickschen & Kramm (1998*b*) estimated a depth interval of ∼50–70 km for the pyroxenite precipitation by estimating temperatures and pressures for the host peridotite using the two-pyroxene geothermometer of Brey & Köhler (1990) in combination with the Ca-olivine–clinopyroxene geo-thermobarometer of Köhler & Brey (1990). The relatively high pressures obtained (1·7–2·2 GPa) are still 0·1–0·5 GPa lower than the corresponding maximum pressures of the stability of the Cr-bearing spinel in these peridotites (Witt-Eickschen & Kramm, 1998*b*).

Micaceous hornblendite veins

Small (< 1·5 cm) veins consisting of Ti-rich pargasite (up to 3·8 wt % TiO_2) and phlogopite occur exclusively in contact with the equigranular recrystallized peridotites from shallow mantle depths (Fig. 2f). As a result of the interaction with the vein melts the geochemical and isotopic characteristics of the peridotitic wall rocks were altered in a transition area of a very limited distance of ∼1 cm from the vein contact. Within this area LREE, Sr and Nb were 'leached' from, whereas Ti, Zr and Hf were added into the wall rock, and the $^{87}Sr/^{86}Sr$ ratio of the host peridotite changed towards the values of the hornblendite vein (Witt-Eickschen *et al.*, 1998).

TRACE ELEMENT CHARACTERISTICS AND Sr–Nd–Pb ISOTOPE SIGNATURES OF THE XENOLITHS

Modally metasomatized xenoliths with texturally equilibrated Ti-poor amphiboles

Amphibole and clinopyroxene from the equigranular recrystallized xenoliths are strongly enriched in the LREE and middle REE (MREE) and relatively
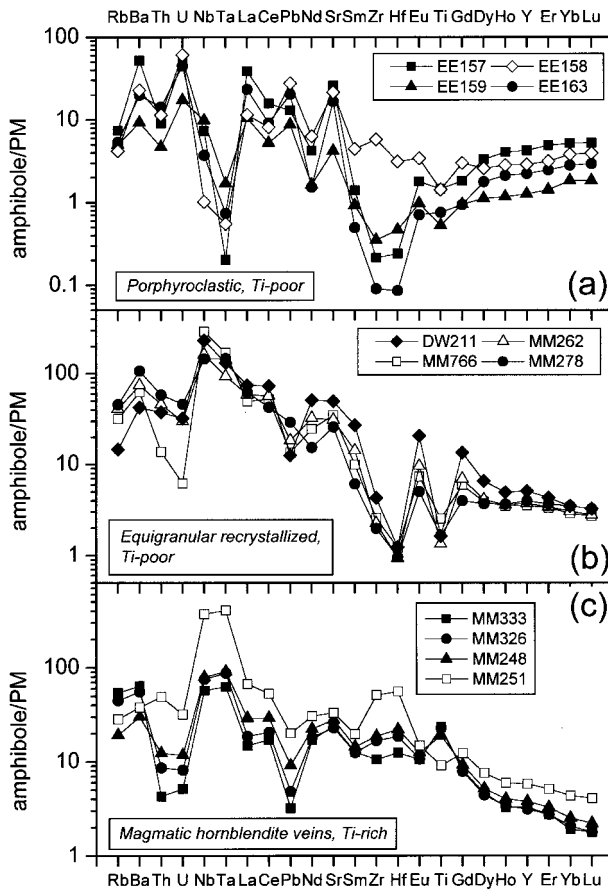
Fig. 3. Trace element patterns [normalized to the primitive mantle (PM) values of Hofmann (1988)]: Ti-poor amphiboles from (a) porphyroclastic and (b) equigranular recrystallized peridotite xenoliths; (c) Ti-rich amphiboles from magmatic hornblendite veins. DW, Dreiser Weiher; MM, Meerfelder Maar; EE, East Eifel.
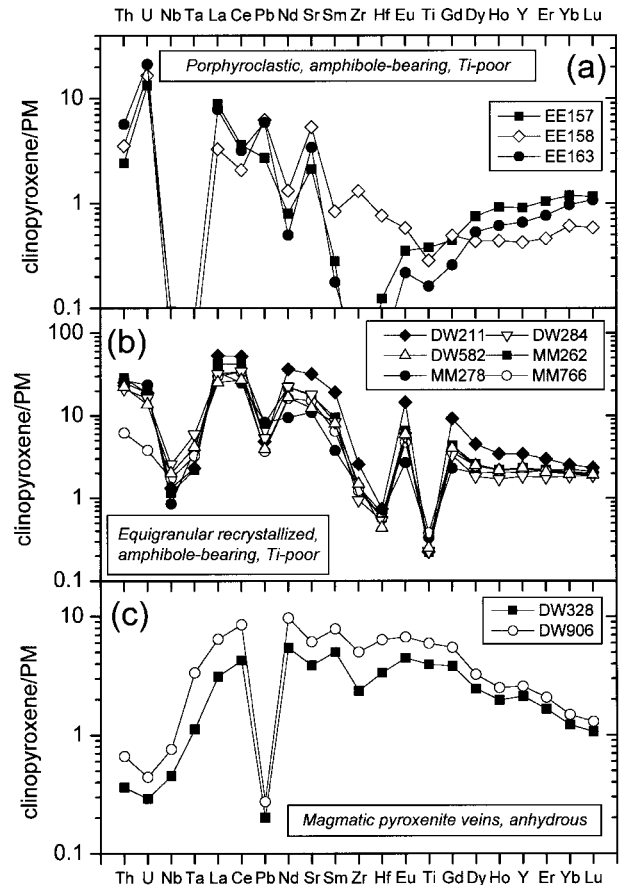
Fig. 4. Trace element patterns of clinopyroxene from (a) amphibole-bearing porphyroclastic and (b) equigranular recrystallized peridotites, and (c) anhydrous magmatic clinopyroxenite veins.

depleted in the HFSE Ti, Zr, and Hf (Figs 3b and 4b). In contrast, the concentrations of the highly incompatible HFSE Nb and Ta are extremely high in the amphibole, resulting in $(Nb/La)_n$ and $(Ta/La)_n$ ratios of 2–6 and 2–3, respectively. With the exception of one sample (MM278), amphibole and clinopyroxene reveal a trough for Pb relative to REE.

The REE patterns of amphibole (Fig. 3a) and clinopyroxene (Fig. 4a) from the porphyroclastic xenoliths display a continuous decrease from Lu to Dy and range from V-shaped with minima at Sm, Eu or Gd to moderately enriched in both LREE and MREE. Compared with the pargasites from the equigranular recrystallized xenoliths, the amphiboles have lower K contents (Table 2), a strong depletion of Nb and Ta relative to REE [$(Nb/La)_n < 1$], higher concentrations of Ba, Sr, Pb and U relative to REE (Fig. 3a), and distinctly higher U/Th ratios.

The Sr–Nd isotope compositions of coexisting clinopyroxene and Ti-poor amphibole are indistinguishable

(MM766 in Table 4) and plot in an Sr–Nd isotope diagram significantly below the field for the primitive Cenozoic Eifel volcanic rocks (Fig. 5). The positively correlated $^{208}Pb/^{204}Pb$ and $^{206}Pb/^{204}Pb$ ratios define a linear array indicating that the time-integrated Th/U ratio in the source of the metasomatic agents was higher than that for ocean island basalts (OIB) from the northern hemisphere (Fig. 6a). A less coherent but stronger trend away from the Northern Hemisphere Reference Line (NHRL) of Hart (1984) is seen in the $^{207}Pb/^{204}Pb$ vs $^{206}Pb/^{204}Pb$ diagram (Fig. 6a).

Broad positive and negative correlations, respectively, exist between $^{206}Pb/^{204}Pb$ and $^{143}Nd/^{144}Nd$ and $^{87}Sr/^{86}Sr$ (Fig. 7). The data plot between the two end-member mantle components EM1 and HIMU that define the LoNd ('low Nd') array of Hart et al. (1986). The strongest isotopic influence of a HIMU-like component is manifested in the equigranular recrystallized xenoliths from the Dreiser Weiher (samples DW194, DW211). Clinopyroxenes from these samples have $^{206}Pb/^{204}Pb$ ratios of >20 that fall on or
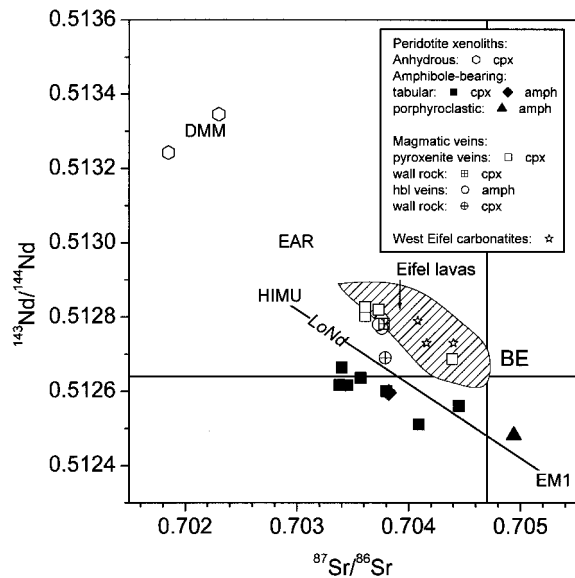
Fig. 5. Comparison of Sr–Nd isotope compositions between clinopyroxenes and amphiboles from anhydrous and hydrous peridotites, magmatic veins and adjacent periditic wall rocks and Cenozoic primitive lavas (Kramers *et al.*, 1981; Wörner *et al.*, 1986) and extrusive carbonatites from the Eifel (Riley *et al.*, 1999). BE, bulk silicate Earth; LoNd, 'low Nd' array (Hart *et al.*, 1986); EAR, European Asthenospheric Reservoir (Cebriá & Wilson, 1995).

close to the NHRL in the Pb–Pb isotope covariation diagrams (Fig. 6). Rosenbaum & Wilson (1996) reported similar high $^{206}Pb/^{204}Pb$ ratios for xenoliths from another West Eifel locality. The amphiboles from the porphyroclastic xenolith from the East Eifel plot closer towards the isotopic end-member EM1 along the EM1–HIMU trend (Fig. 7).

Clinopyroxenite and hornblendite magmatic veins

Discrete, 10–16 cm diameter clinopyroxenite xenoliths (DW906, DW918) and 2–5 cm wide clinopyroxenite veins of composite xenoliths (DW327, DW328) from depths of ~50–70 km were selected for the Pb isotope study. Their clinopyroxenes display convex-upward REE patterns and troughs for HFSE and Sr (Witt-Eickschen & Kramm, 1998*b*). The Pb, Th and U concentrations are significantly lower (Fig. 4c) compared with the clinopyroxenes from the porphyroclastic and equigranular recrystallized peridotites (Fig. 4a and b).

The Ti-rich amphiboles from relatively wide hornblendite veinlets (~1 cm) occurring in contact with the hydrous equigranular recrystallized host peridotites from shallower mantle depths display convex-upward REE patterns combined with high HFSE concentrations and significant troughs for Th, U and Pb relative to REE (Fig. 3c). Ti-rich amphibole from a very thin hornblendite veinlet (<2 mm in size) has
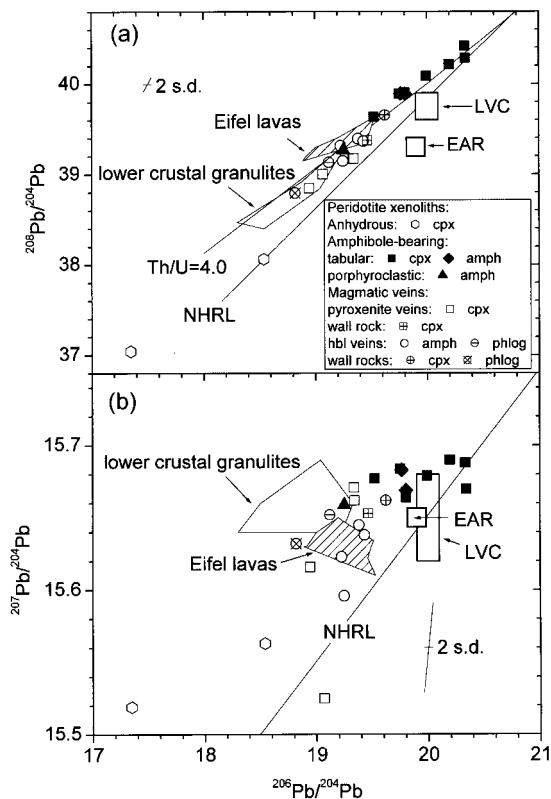

Fig. 6. Comparison of Pb isotope compositions between clinopyroxene, amphibole and phlogopite from mantle xenoliths, Cenozoic lavas (Wörner *et al.*, 1986; Wedepohl & Baumann, 1999) and lower-crustal xenoliths from the Eifel (Rudnick & Goldstein, 1990). NHRL, Northern Hemisphere Reference Line (Hart, 1984); EAR [European Asthenospheric Reservoir of Cebriá & Wilson (1995)] and LVC [Low-Velocity Component of Hoernle *et al.* (1995)] represent a sub-lithospheric geochemically uniform source for volcanic rocks in a region extending from the eastern Atlantic to central Europe and the western Mediterranean.

an REE pattern with a steep negative slope from LREE to heavy REE (HREE) combined with very high Nb, Zr and Hf concentrations (sample MM251 in Fig. 3c; not analysed for Sr–Nd–Pb isotopes because of the small vein volume). This veinlet has been interpreted to represent virtually complete crystallization of small volumes of melt that formed the amphiboles present in the other veins (Witt-Eickschen *et al.*, 1998).

Despite the significant mineralogical and geochemical differences between the clinopyroxenite and hornblendite veins, the two types of magmatic veins are isotopically similar, suggesting a genetic link between their parental melts (Table 4). The Sr–Nd isotopic characteristics of the hornblendite veins are identical and lie within the range obtained for the clinopyroxenite veins (Fig. 5). The $^{206}Pb/^{204}Pb$ (18·95–19·43), $^{207}Pb/^{204}Pb$ (15·53–15·67) and $^{208}Pb/^{204}Pb$ ratios (38·85–39·39) of vein clinopyroxene, amphibole and phlogopite cover, within the limits of error, the entire
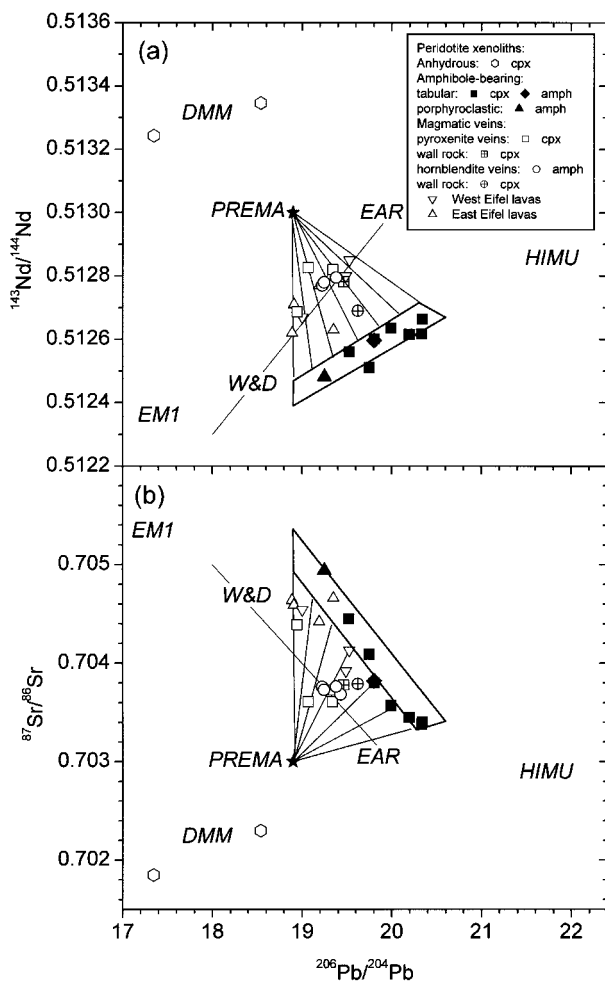
Fig. 7. Comparison of Sr–Nd–Pb isotope compositions between mantle xenoliths and Cenozoic lavas from the Eifel (Wörner *et al.*, 1986; Wedepohl & Baumann, 1999). The bold outlines mark the 'HIMU–EM1 array' created by the modally metasomatized xenoliths; the fine lines mark the interaction of asthenospheric PREMA- or EAR-like melts with components derived from the heterogeneous EM1–HIMU-like lithospheric mantle. The 'W&D line' of Wilson & Downes (1991) represents mixing of uniform asthenospheric HIMU–DMM-like (EAR) and lithospheric EM1-like material. End-member components from Hart *et al.* (1992) and PREMA (prevalent mantle) component of Wörner *et al.* (1986).

range observed for the Cenozoic lavas from the Eifel volcanic field (Fig. 6). The vein and wall-rock minerals plot off the HIMU–EM1 trend shown by the hydrous peridotite xenoliths within the DMM–HIMU–EM1 space in the Sr–Nd–Pb diagrams (Fig. 7).

High-temperature, LREE-depleted xenoliths

Clinopyroxene from the most fertile LREE-depleted lherzolite with respect to mineralogy (DWK1: 10 wt % cpx) has the lowest Pb concentration (20 ppb) and the most unradiogenic Pb isotope composition (^{206}Pb/

^{204}Pb ~17·3) of all investigated clinopyroxene samples. It represents depleted mantle material with Sr–Nd–Pb isotope signatures similar to DMM that defines the source region of mid-ocean ridge basalts from the North Atlantic. The Pb isotope composition of clinopyroxene from the other high-temperature xenolith (DW58) is more radiogenic and plots in the ^{208}Pb/^{204}Pb vs ^{206}Pb/^{204}Pb covariation diagram on the NHRL (Fig. 6a). This supports the conclusion of Stosch & Lugmair (1986) that this peridotite may have experienced old (>1·1 Ga) multi-stage enrichment and depletion processes.

DISCUSSION

Nature of the metasomatic agents: evidence from trace element compositions

Porphyroclastic xenoliths

The strong depletion from HREE to MREE in the clinopyroxenes and amphiboles (Figs 3a and 4a) of the porphyroclastic xenoliths suggests that these peridotites were initially depleted in their incompatible trace element abundances. During the enrichment process elements fairly soluble in aqueous fluids such as the LILE (Ba, Sr) and Pb have been added to the clinopyroxenes and amphiboles as manifested by their high Pb/Ce and Sr/Sm ratios, whereas Ta and Nb concentrations are depleted relative to U, REE and LILE (Figs 3a and 4a). The solubility of Th in aqueous fluids is lower than that of U at high oxygen fugacities (fO_2 > FMQ – 2, where FMQ is fayalite–magnetite–quartz) and the resulting excess of U in the fluids can be further enhanced during the transit through the upper mantle (e.g. Brenan *et al.*, 1995). Thus, the elevated primitive mantle normalized U/Th ratios in the amphiboles (3·1–5·9) and clinopyroxenes (2·7–5·5) from the porphyroclastic xenoliths compared with those from the equigranular recrystallized peridotites and magmatic veins (U/Th 0·4–1·3) are also compatible with a hydrous metasomatic agent. The remarkable amounts of W and Mo (0·1–0·9 ppm W; 0·5–1·2 ppm Mo) found in the amphiboles and clinopyroxenes (Tables 2 and 3) provide additional evidence for the involvement of aqueous fluids. These highly incompatible siderophile elements are commonly mobilized by aqueous fluids, as can be inferred from the composition of black smokers and hydrothermal ore-deposits and from melt–aqueous fluid partition coefficients (Keppler & Wyllie, 1991).

Equigranular recrystallized xenoliths

The element patterns and Sr–Nd–Pb isotope compositions of clinopyroxene and amphibole in the equigranular recrystallized xenoliths from the West Eifel are
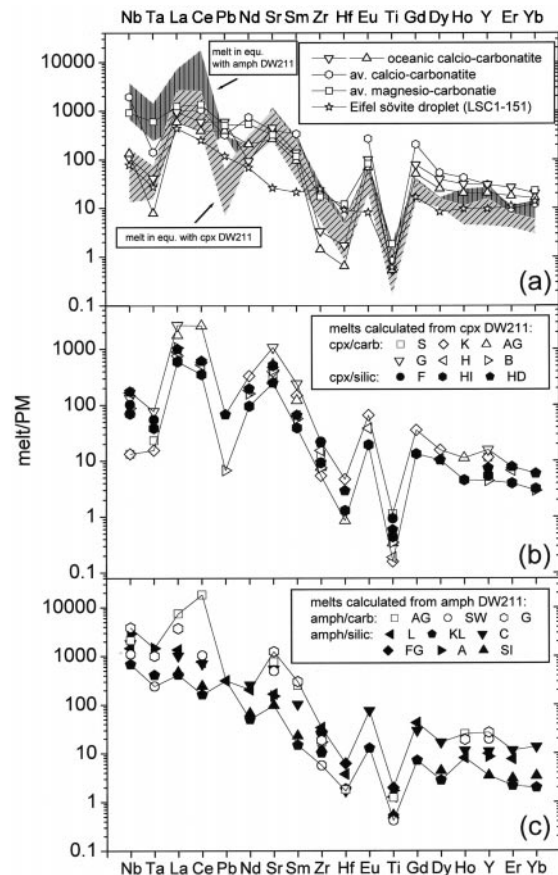
Fig. 8. Comparison of trace element patterns between oceanic (Hoernle *et al.*, 2002), continental (Woolley & Kempe, 1989) and East Eifel carbonatites (Liebsch, 1996) and hypothetical melts (a) in equilibrium with clinopyroxene (b) and amphibole (c) of sample DW211, which were calculated by using different sets of mineral–melt partition coefficients (Table 5).

distinctly different from those of the minerals from the magmatic vein systems and at variance with an origin by spatially limited wall-rock reaction postulated by other workers (e.g. Nielson & Wilshire, 1993). Hence this type of mantle metasomatism may be related to pervasive melt flow through a porous medium rather than to wall-rock reactions.

Rare extrusive Quaternary carbonatitic and calcite-bearing rocks from the West and East Eifel (Liebsch *et al.*, 1996; Riley *et al.*, 1999) point to the existence of carbonatitic melts in the underlying lithosphere of the Eifel as their Sr–Nd isotope systematics are consistent with a mantle origin (Fig. 5). Thus we evaluated whether melts parental to carbonatites might be responsible for the enrichment in the peridotites by calculating the trace element concentrations of the hypothetical metasomatic agents in equilibrium with the equigranular recrystallized mantle xenoliths. Representative trace element patterns of the hypothetical melts, shown in Fig. 8, were calculated from the

trace element compositions of amphibole (Fig. 3b) and clinopyroxene (Fig. 4b) from sample WE211, which has a highly radiogenic Pb isotope signature. For the calculation different sets of mineral–silicate melt and mineral–carbonatitic melt partition coefficients from the literature were used (Table 5). The metasomatic agents in equilibrium with clinopyroxene and amphibole are enriched in LREE and Sr and reveal marked negative anomalies of Ti, Zr and Hf relative to REE (Fig. 8b and c). Their trace element compositions are very similar to those of oceanic carbonatites (Fig. 8a) attributed to an asthenospheric mantle origin (Hoernle *et al.*, 2002). In contrast, the Eifel carbonatites, which are petrogenetically linked to the Quaternary silicate Eifel lavas (e.g. Laacher See sövite shown in Fig. 8a; Liebsch, 1996), lack the relative Sr enrichment. Other marked features of the calculated melts are the Nb/Ta (on average 37) and Zr/Hf (on average 269) ratios distinctly higher and Ti/Eu (on average 130) ratios lower than the primitive mantle values (17·6, 34·2 and 7452, respectively), which are also consistent with the trace element characteristics of carbonatites (e.g. Woolley & Kempe, 1989). Because of their low viscosity and low dihedral wetting angles, carbonatitic melts can escape their source regions at melt fractions as low as 0·1% and percolate upwards through the peridotite matrix as a result of formation of interconnected grain-edge networks (e.g. Minarik, 1998). Thus such melts are considered as very effective and mobile metasomatic agents in the lithospheric mantle (e.g. Yaxley *et al.*, 1998). The petrography and major element chemistry of the equigranular recrystallized peridotites, however, provide no further support for a carbonatite-induced metasomatism. This makes the interpretation considering interaction of the peridotites with carbonatitic melts difficult, but does not preclude this possibility.

Clinopyroxenite and hornblendite veins

The clinopyroxene from the clinopyroxenite and the amphibole from the hornblendite veins differ significantly from those in the metasomatized peridotite host rocks by their higher Ti concentrations and convex-upward REE patterns (Figs 3 and 4) that are typical for amphibole and clinopyroxene megacrysts precipitated from basic melts (Irving & Frey, 1984). Thus the new trace element data obtained by LA-ICP-MS for selected veins support our previous conclusions (Witt-Eickschen & Kramm, 1998b; Witt-Eickschen *et al.*, 1998) that the melts from which the clinopyroxenite and hornblendite veinlets crystallized clearly have a silicate melt origin. Using experimental mineral–silicate melt partition coefficients (Table 5) yields trace element compositions for a hypothetical melt in equilibrium with vein clinopyroxene DW906 (Table 3) perfectly overlapping in its shape with those of the Eifel

Table 5: Mineral–melt partition coefficients from the literature used to calculate the hypothetical melts shown in Figs 8 and 9

	cpx–carbonatite melt						cpx–silicate melt			
	AG	B	G	H	K	S	F	HD	HH	HI
Nb	0·017	0·02	0·01	0·008	0·1	0·1	0·013	0·0077		0·019
Ta			0·03		0·15	0·1	0·042			0·06
La	0·03	0·05	0·02	0·06	0·07			0·0536	0·06	0·089
Ce	0·02			0·1	0·09			0·0858	0·10	0·148
Pb		0·93						0·072		
Nd		0·26		0·2	0·11			0·1873	0·20	0·38
Sr	0·06	0·08	0·03	0·13	0·08	0·1		0·1283		0·063
Sm	0·16	0·35	0·08	0·3	0·13			0·291	0·30	0·49
Zr	0·34	0·78	0·29	0·17	0·48	0·2	0·117	0·1234	0·17	0·283
Hf	0·88				0·16			0·256		0·58
Eu				0·38	0·22				0·38	0·75
Ti	0·66	0·72		1·2	1·42	0·2	0·24	0·384	0·35	0·512
Gd					0·26				0·40	0·7
Dy				0·44	0·29			0·442	0·44	
Ho	0·31									0·77
Y		0·89	0·22		0·30	0·3		0·467		0·64
Er				0·45	0·41			0·387	0·45	0·76
Yb		0·96						0·43	0·45	0·8

	amph–carbonatite melt			amph–silicate melt						
	AG	G	SW	A	AGR	C	FG	KL	L	SI
Nb	0·11	0·06	0·21	0·08		0·126		0·34	0·159	
Ta		0·13	0·54	0·09				0·32		
La	0·01	0·02			0·12	0·073		0·18	0·055	0·16
Ce	0·004		0·07			0·104		0·45	0·096	0·3
Pb									0·04	
Nd						0·2		1·02	0·25	0·77
Sr	0·065	0·04	0·10	0·33	0·25	0·093			0·298	0·51
Sm	0·108	0·09			0·46	0·265		1·83		1·18
Zr	0·25	0·23	0·76	0·25		0·188	0·15	0·42	0·127	0·35
Hf	0·69					0·733	0·2	0·66	0·33	
Eu						0·277		1·62		
Ti	1·32		3·9	0·95	1·24		0·83	3·2	1·29	3·06
Gd						0·463		1·9	0·32	
Dy						0·395		2·37		1·52
Ho	0·199	0·26			0·51	0·432			0·62	
Y	0·19	0·19	0·26	0·6		0·463			0·52	1·47
Er						0·373		2·01	0·57	1·44
Yb						0·257		1·77		1·03

A, Adam *et al*. (1993); AG, Adam & Green (2001); AGR, Adam & Green (1994); B, Blundy & Dalton (2000); C, Chazot *et al*. (1996); F, Forsythe *et al*. (1994); FG, Fujinawa & Green (1997); G, Green *et al*. (1992); H, Hauri *et al*. (1993); HD, Hart & Dunn (1993); HH, Hauri & Hart (1994); HI, Hill *et al*. (2000); K, Klemme *et al*. (1995); KL, Klein *et al*. (1997); L, LaTourette *et al*. (1995); S, Sweeney *et al*. (1995); SI, Sisson (1994); SW, Sweeney *et al*. (1992).
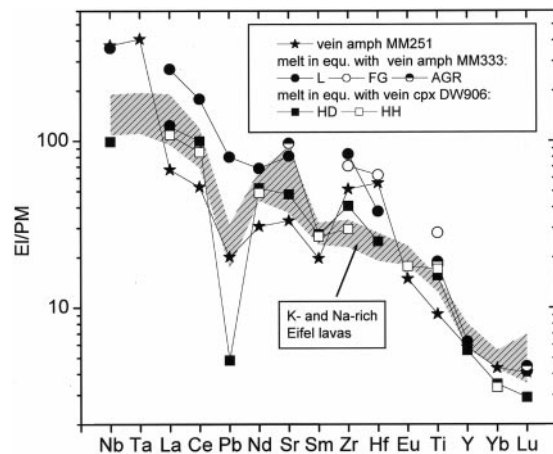
Fig. 9. Comparison of trace element patterns between K- and Na-rich Eifel lavas (Wedepohl *et al.*, 1994; H. G. Stosch & W. Bausen, unpublished data, 2000), vein amphibole MM251 (representing complete crystallization of small volumes of melt) and hypothetical melts in equilibrium with magmatic clinopyroxenite (DW906) and hornblendite (MM333) veins calculated by using different sets of partition coefficients (Table 5).

silicate volcanic rocks (Fig. 9). The melt pattern calculated from the composition of vein amphibole MM333 as well as the pattern of vein amphibole MM251, representing complete crystallization of a small volume of melt (Witt-Eickschen *et al.*, 1998), display a significant enrichment of Zr and Hf over Sm not recognized in the Eifel lavas.

Metasomatic events in the lithospheric mantle beneath the Eifel: constraints from the Sr–Nd–Pb isotope signatures

Formation of a heterogeneous EM1–HIMU lithosphere

The combined Sr–Nd–Pb isotopic signatures of the mantle xenoliths display a large range of variations indicating isotopic heterogeneity in the lithospheric mantle underneath the Eifel (Table 4; Fig. 7). A DMM component occurs as an old protolith in the LREE-depleted, high-temperature lherzolites from the deeper regions of the Eifel lithosphere. These xenoliths may represent former asthenospheric material although there is no textural evidence for this conclusion. In contrast, the Sr–Nd–Pb isotope and trace element compositions of the hydrous tabular recrystallized and porphyroclastic peridotites provide evidence that highly enriched components infiltrated the initially depleted shallow continental mantle lithosphere, which might be related to the Cenozoic volcanism. According to current hypotheses (Wilson & Downes, 1991; Cebriá & Wilson, 1995; Hoernle *et al.*, 1995) the Cenozoic primitive magmas of the continental volcanism in western and central Europe are

thought to represent two distinct mantle sources. The most primitive sodium-rich mafic lavas from the Cenozoic European volcanic fields, as well as from the contemporaneous magmatism in the western Mediterranean and eastern Atlantic, have a common mantle source variously referred to as the EAR (European Asthenospheric Reservoir) or LVC (Low Velocity Composition) located deep in the asthenospheric mantle with isotope characteristics plotting between DMM and HIMU. Potassium-rich basalts have been attributed to EM1-like sources reflecting small-degree melts derived from phlogopite- (± amphibole)-rich parts of the lithospheric mantle whose variable isotope composition corresponds to the local tectono-magmatic history (e.g. Wilson & Downes, 1991). In the Quaternary Eifel volcanic fields both types of lavas occur: an Na-rich ($K_2O/Na_2O < 0.5$) olivine nephelinite and basanite suite recording Sr–Nd–Pb similar to, but less extreme than the EAR source and a K-rich ($K_2O/Na_2O > 0.5$) leucitite–melilite–nephelinite suite with Sr–Nd isotopic characteristics close to Bulk Earth (Kramers *et al.*, 1981; Wörner *et al.*, 1986).

However, on the basis of our data there is no indication of the involvement of the EAR component during the HIMU–EM1-like enrichment of the shallow subcontinental lithosphere manifested in the hydrous mantle xenoliths (Fig. 7). Thus the metasomatic agents responsible for this enrichment event do not have their isotopic equivalent in the young alkaline magmatism of Europe. Rosenbaum & Wilson (1996) proposed a two-stage enrichment model for the Eifel mantle: (1) subduction modification of a mantle protolith; (2) a later enrichment by asthenosphere-derived melts. Mantle xenoliths with an EM1-like isotopic signature occur in both the East Eifel (this study) and West Eifel (Rosenbaum & Wilson, 1996) volcanic fields, implying a relatively large-scale metasomatic event. The mobilization of the volatile-rich EM1-like fluids is temporally linked with a deformation process in the shallow lithospheric mantle (Witt & Seck, 1989). This suggests that fluids carrying an isotope component from a crustal source might be related to a major tectonic episode in this area, i.e. the Hercynian orogeny (Rosenbaum & Wilson, 1996). Evidence for an episode of subduction beneath the Eifel area in the Hercynian orogeny is provided by the Sr–Nd–Pb isotope signatures of amphibole-bearing granulites sampled from Quaternary tephra deposits of the East Eifel volcanic field. These granulites are considered to occupy the base of the East Eifel crust down to a Moho depth of 29–34 km (Okrusch *et al.*, 1979) and exhibit EM1-like present-day Nd–Pb isotope signatures (Loock *et al.*, 1990; Rudnick & Goldstein, 1990). Rudnick & Goldstein (1990) attributed their formation to underplating of mantle-derived basaltic magmas that mixed with

material in the pre-existing Precambrian lower crust $\sim$450 Myr ago. A protolith age of $\sim$400 Ma is recorded by amphibolite-facies metagranodiorites from $\sim$10–20 km under the Eifel that formed by partial melting of a lower-crustal source (Stosch *et al.*, 1992). Rudnick & Goldstein (1990) explained the discrepancy between the Proterozoic Nd model ages of the granulites ($\sim$1·5 Ga; Stosch *et al.*, 1986) and their much younger age of 450 Ma inferred from the Pb isotope compositions by a tectonic transport of upper-crustal lithologies into the lower crust during the Variscan orogeny. The Sr–Nd–Pb isotope signature of some granulite xenoliths was not reset by infiltration of melts or fluids associated with the Cenozoic magmatic event (Stosch *et al.*, 1992). Thus the isotopic EM1-like signature seems to be a primary feature of the Hercynian lower crust and possibly also of the lithospheric mantle into which mafic mantle-derived lavas intruded later.

If EM1-like subduction-related fluids affected the initially LREE-depleted lithospheric mantle, this requires a second stage of enrichment by melts with HIMU-like isotope signatures that reacted during their ascent with the EM1-like subcontinental mantle lithosphere. This process resulted in small-scale isotopic heterogeneities within the metasomatized upper mantle characterized by varying EM1–HIMU-like isotope signatures. The most extreme (i.e. radiogenic) $^{206}Pb/^{204}Pb$ and $^{208}Pb/^{204}Pb$ isotope ratios in the West Eifel mantle xenoliths are unique for the European lithospheric mantle (Downes, 2001). The HIMU signature is even stronger than that of the uniform EAR or LVC endmember composition postulated for the Cenozoic European and eastern Atlantic volcanic provinces (Fig. 6). Xenoliths with the most radiogenic Pb isotope compositions converge in the $^{207}Pb–^{206}Pb$ covariation diagram on the NHRL (Fig. 6b), which represents a 1·77 Ga secondary isochron for oceanic basalts. However, the provenance of the HIMU-like metasomatic agent is unconstrained: it may be either plume derived or an unrelated ancient metasomatic component incorporated into ageing continental lithosphere. In addition, the timing of the melt infiltration remains uncertain and several geodynamic scenarios seem to be possible: (1) the input of the HIMU-like component into the mantle lithosphere is relatively old and associated with the Hercynian orogeny. (2) The metasomatic agents record the very low-degree partial melts initiated by an early Cretaceous deep-sourced mantle plume (Wilson, 1996) with a HIMU-like signature such as the ocean island basalts of St. Helena. (3) The fluid mobilization is young. It began shortly before the main volcanism in the Cenozoic and may be due to the upwelling of a small-scale mantle 'hot-blob' from a layer deeper than 400 km (Ritter *et al.*, 2001). Alternatively, the fluid

generation may have started during early stages of rifting in connection with the collision of the African and European plates. This requires a reactivation of subducted old crustal domains that may have been deposited at the base of the 'post-Hercynian' lithosphere.

On the other hand, the well-developed HIMU–EM1 trend may be the result of source heterogeneity, rather than mixing of metasomatic agents from isotopically distinct mantle reservoirs. Bell & Tilton (2001) considered that both HIMU and EM1 sources are stored within the deep mantle and attributed the formation of an EM1–HIMU-like mantle lithosphere beneath East Africa (Cohen *et al.*, 1984) to the addition of material from a heterogeneous mantle plume covering the complete isotope spectrum between HIMU and EM1 signatures. Thus melting of isotopically distinct mantle domains in a heterogeneous uprising mantle plume could have produced all the metasomatic agents responsible for the HIMU–EM1 enrichment in the deformed mantle lithosphere beneath the Eifel.

Vein metasomatism by young EM1–DMM–HIMU basaltic melts

Witt-Eickschen *et al.* (1998) inferred from textural, geochemical and Sr–Nd-isotopic evidence that the highly LREE-enriched amphibole grains of tabular habit present in the equigranular recrystallized peridotite wall rocks adjacent to the hornblendite veins formed during an episode of modal metasomatism pre-dating the vein melt injection. As a consequence of the subsequent vein metasomatic event new amphiboles precipitated in some host peridotites. These are, in contrast to the pre-existing amphiboles, not in textural equilibrium with the constituent phases and have chemical compositions similar to the Ti-rich vein amphiboles (Witt-Eickschen *et al.*, 1993). In addition, small-scale compositional gradients within the pre-existing individual Ti-poor amphibole grains developed (Witt-Eickschen *et al.*, 1993) that were used to estimate time constraints for the vein formation (Witt-Eickschen *et al.*, 1998) by applying the diffusion-controlled chromatographic fractionation model of Bodinier *et al.* (1990). The trace element modelling of these zoning profiles in the tabular amphiboles implies an extremely brief event of melt–wall-rock interaction, which occurred within a time interval of only 10–1000 years before the rapid transport of the xenoliths to the surface (Witt-Eickschen *et al.*, 1998). Thus the vein metasomatism established in the composite xenoliths represents the brief final stage of the multiple enrichment processes beneath the Eifel, obviously as a consequence of the Cenozoic volcanism.

The present isotope study supports this view of a young vein metasomatic event, as the Sr–Nd–Pb data

of the minerals from the magmatic clinopyroxenite and hornblendite veins and from their peridotitic wall rocks and the Quaternary Eifel lavas share nearly the same diversity of Sr–Nd–Pb isotopic signatures (Fig. 7). This indicates common sources for the young Eifel volcanism and for the melts parental to the veins that migrated upwards through a system of dyke networks during their ascent through the mantle lithosphere. Because a DMM-like or PREMA-like component is completely lacking in the EM1–HIMU-like metasomatic agents that have pre-enriched the shallower subcontinental Eifel mantle, the mobilization of the DMM–HIMU–EM1 material recognized in the young lavas occurred at the earliest in the Tertiary, contemporaneously with the development of the extensive rift system in Europe and the main melt generation. The diversity of the isotope signatures recorded by the Eifel lavas and the vein melts genetically related to the young Eifel volcanism can have been produced by the interaction of the primary asthenospheric PREMA- or EAR-like melts with components derived from the highly heterogeneous EM1–HIMU-like lithospheric mantle (Fig. 7).

REFERENCES

Adam, J. & Green, T. H. (1994). The effects of pressure and temperature on the partitioning of Ti, Sr and REE between amphibole, clinopyroxene and basanitic melts. *Chemical Geology* **117**, 219–233.

Adam, J. & Green, T. (2001). Experimentally derived partition coefficients for minor and trace elements in peridotite minerals and carbonatitic melt, and their relevance to natural carbonatites. *European Journal of Mineralogy* **13**, 815–827.

Adam, J., Green, T. H. & Sie, S. H. (1993). Proton microprobe determined partitioning of Rb, Sr, Ba, Y, Zr, Nb and Ta between experimentally produced amphiboles and silicate melts with variable F content. *Contributions to Mineralogy and Petrology* **109**, 29–49.

Bell, K. & Tilton, G. R. (2001). Nd, Pb and Sr isotopic compositions of East African carbonatites: evidence for mantle mixing and plume inhomogeneity. *Journal of Petrology* **42**, 1927–1945.

Blundy, J. & Dalton, J. (2000). Experimental comparison of trace element partitioning between clinopyroxene and melt in carbonate and silicate systems, and implications for mantle metasomatism. *Contributions to Mineralogy and Petrology* **139**, 356–371.

Bodinier, J. L., Vasseur, G., Vernière, J., Dupuy, C. & Fabriès, J. (1990). Mechanisms of mantle metasomatism: geochemical evidence from the Lherz orogenic peridotite. *Journal of Petrology* **31**, 597–628.

Brenan, J. M., Shaw, H. F., Ryerson, F. J. & Phinney, D. L. (1995). Mineral–aqueous fluid partitioning of trace elements at 900°C and 2·0 GPa: constraints on the trace element chemistry of mantle and deep crustal fluids. *Geochimica et Cosmochimica Acta* **59**, 3331–3350.

Brey, G. P. & Köhler, T. (1990). Geothermobarometry in four-phase lherzolites II. New thermobarometers and practical assessment of existing thermobarometers. *Journal of Petrology* **31**, 1353–1378.

Cebriá, J. M. & Wilson, M. (1995). Cenozoic mafic magmatism in Western/Central Europe: a common European asthenospheric reservoir? *Terra Abstracts* **7**, 162.

Chazot, G., Menzies, M. A. & Harte, B. (1996). Determination of partition coefficients between apatite, clinopyroxene, amphibole, and melt in natural spinel lherzolites from Yemen: implications for wet melting of the lithospheric mantle. *Geochimica et Cosmochimica Acta* **60**, 423–437.

Cohen, R. S., O'Nions, R. K. & Dawson, J. B. (1984). Isotope geochemistry of xenoliths from East Africa: implications for development of mantle reservoirs and their interaction. *Earth and Planetary Science Letters* **68**, 209–220.

Downes, H. (2001). Formation and modification of the shallow subcontinental lithospheric mantle: a review of geochemical evidence from ultramafic xenolith suites and tectonically emplaced ultramafic massifs of western and central Europe. *Journal of Petrology* **42**, 233–250.

Eggins, S. M., Rudnick, R. L. & McDonough, W. F. (1998). The composition of peridotites and their minerals: a laser-ablation ICP-MS study. *Earth and Planetary Science Letters* **154**, 53–71.

Forsythe, L. M., Nielson, R. L. & Fisk, M. R. (1994). High-field-strength element partitioning between pyroxene and basaltic to dacitic magmas. *Chemical Geology* **117**, 107–125.

Fujinawa, A. & Green, T. H. (1997). Partitioning behaviour of Hf and Zr between amphibole, clinopyroxene, garnet and silicate melts at high pressure. *European Journal of Mineralogy* **9**, 379–391.

Granet, M., Wilson, M. & Achauer, U. (1995). Imaging a mantle plume beneath the Massif Central (France). *Earth and Planetary Science Letters* **136**, 281–296.

Green, T. H., Adam, J. & Sie, S. H. (1992). Trace element partitioning between silicate minerals and carbonatite at 25 kbar and application to mantle metasomatism. *Mineralogy and Petrology* **46**, 179–184.

Hart, S. R. (1984). A large-scale isotope anomaly in the southern hemisphere mantle. *Nature* **309**, 753–757.

Hart, S. R. & Dunn, T. (1993). Experimental cpx/melt partitioning of 24 trace elements. *Contributions to Mineralogy and Petrology* **113**, 1–8.

Hart, S. R., Gerlach, D. C. & White, W. M. (1986). A possible new Sr–Nd–Pb mantle array and consequences for mantle mixing. *Geochimica et Cosmochimica Acta* **50**, 1551–1557.

Hart, S. R., Hauri, E. H., Oschmann, L. A. & Whitehead, J. A. (1992). Mantle plumes and entrainment: isotopic evidence. *Science* **256**, 517–520.

Hauri, E. H. & Hart, S. R. (1994). Constraints on melt migration from mantle plumes: a trace element study of peridotite xenoliths from Savai'i, Western Samoa. *Journal of Geophysical Research* **99**(B12), 24301–24321.

Hauri, E. H., Shimizu, N., Dieu, J. J. & Hart, S. R. (1993). Evidence for hotspot-related carbonatite metasomatism in the oceanic upper mantle. *Nature* **365**, 221–227.

Hegner, E., Walter, H. J. & Satir, M. (1995). Pb–Sr–Nd isotopic compositions and trace element geochemistry of megacrysts and melilitites from the Tertiary Urach volcanic field: source composition of small volume melts under SW Germany. *Contributions to Mineralogy and Petrology* **122**, 322–335.

Hill, E., Wood, B. J. & Blundy, J. D. (2000). Effect of calcium-tschermaks component on trace element partitioning between clinopyroxene and silicate melt. *Lithos* **53**, 203–215.

Hoernle, K., Zhang, Y. S. & Graham, D. (1995). Seismic and geochemical evidence for large-scale mantle upwelling beneath the eastern Atlantic and western and central Europe. *Nature* **374**, 34–39.

Hoernle, K., Tilton, G., Le Bas, M. J., Duggen, S. & Garbe-Schönberg, D. (2002). Geochemistry of oceanic carbonatites compared with continental carbonatites: mantle recycling of oceanic crustal carbonate. *Contributions to Mineralogy and Petrology* **142**, 520–542.

Hofmann, A. W. (1988). Chemical differentiation of the earth: the relationship between mantle, continental crust and oceanic crust. *Earth and Planetary Science Letters* **90**, 297–314.

Hofmann, A. W. (1997). Mantle geochemistry: the message from oceanic volcanism. *Nature* **385**, 219–229.

Huckenholz, H. G. & Büchel, G. (1988). Tertiärer Vulkanismus der Hocheifel. *Fortschritte der Mineralogie* **66**(Bh2), 43–82.

Irving, A. J. & Frey, F. A. (1984). Trace element abundances in megacrysts and their host basalts: constraints on partition coefficients and megacryst genesis. *Geochimica et Cosmochimica Acta* **48**, 1201–1221.

Kempton, P. D., Fitton, J. G., Saunders, A. D., Nowell, R. N., Taylor, B. S., Hardarson, B. S. & Pearson, G. (2000). The Iceland plume in space and time: a Sr–Nd–Pb–Hf study of the North Atlantic rifted margin. *Earth and Planetary Science Letters* **177**, 255–271.

Keppler, H. & Wyllie, O. J. (1991). Partitioning of Cu, Sn, Mo, W, U, and Th between melt and aqueous fluid in the systems haplogranite–H_2O–HCl and haplogranite–H_2O–HF. *Contributions to Mineralogy and Petrology* **109**, 139–150.

Keyser, M., Ritter, J. R. R. & Jordan, M. (2002). 3D shear-wave velocity structure of the Eifel plume, Germany. *Earth and Planetary Science Letters* **203**, 59–82.

Klein, M., Stosch, H. G. & Seck, H. A. (1997). Partitioning of high field-strength and rare-earth elements between amphibole and quartz-dioritic to tonalitic melts: an experimental study. *Chemical Geology* **138**, 257–271.

Klemme, S., van der Laan, S. R., Foley, S. F. & Günther, D. (1995). Experimentally determined trace and minor element partitioning between clinopyroxene and carbonatite melt under upper mantle conditions. *Earth and Planetary Science Letters* **133**, 439–448.

Köhler, T. & Brey, G. (1990). Calcium exchange between olivine and clinopyroxene calibrated as a geothermobarometer for natural peridotites from 2 to 60 kbar with applications. *Geochimica et Cosmochimica Acta* **54**, 2375–2388.

Kramers, J. D., Betton, P. J., Cliff, R. A., Seck, H. A. & Sachtleben, T. (1981). Sr and Nd isotopic variations in volcanic rocks from the West Eifel and their significance. *Fortschritte der Mineralogie* **59**, 246–247.

LaTourette, T., Hervig, R. L. & Holloway, J. R. (1995). Trace element partitioning between amphibole, phlogopite, and basanite melt. *Earth and Planetary Science Letters* **135**, 13–30.

Liebsch, H. (1996). Die Genese der Laacher See-Karbonatite. Dissertation, Universität Göttingen, 111 pp.

Liebsch, H., Wörner, G. & Oberhänsli, R. (1996). Unmixing and mixing of carbonatite and silicate magma—evidence from Laacher See carbonate-bearing xenoliths. *Journal of Conference Abstracts* **1**, 359.

Loock, G., Stosch, H. G. & Seck, H. A. (1990). Granulite facies lower crustal xenoliths from the Eifel, West Germany: petrological and geochemical aspects. *Contributions to Mineralogy and Petrology* **105**, 25–41.

Mechie, J., Prodehl, C. & Fuchs, K. (1983). The long-range seismic refraction experiment in the Rhenish Massif. In: Fuchs, K., von Gehlen, K., Mälzer, H., Murawski, H. & Semmel, A. (eds) *Plateau Uplift*. Berlin: Springer, pp. 260–275.

Mercier, J. C. & Nicolas, A. (1975). Textures and fabrics of upper mantle peridotites as illustrated by xenoliths from basalts. *Journal of Petrology* **16**, 454–487.

Mertes, H. & Schmincke, H. U. (1985). Mafic potassic lavas of the Quaternary West Eifel volcanic field. *Contributions to Mineralogy and Petrology* **89**, 330–345.

Minarik, W. G. (1998). Complications to carbonate melt mobility due to the presence of an immiscible silicate melt. *Journal of Petrology* **39**, 1965–1973.

Nielson, J. E. & Wilshire, H. G. (1993). Magma transport and metasomatism in the mantle: a critical review of current geochemical models. *American Mineralogist* **78**, 1117–1134.

Norman, M. D., Griffin, W. L., Pearson, N. J., Garcia, M. O. & O'Reilly, S. Y. (1998). Quantitative analysis of trace element abundances in glasses and minerals: a comparison of laser ablation inductively coupled plasma mass spectrometry, solution inductively coupled plasma mass spectrometry, proton microprobe and electron microprobe data. *Journal of Analytical Atomic Spectrometry* **13**, 477–482.

Okrusch, M., Schröder, B. & Schnütgen, A. (1979). Granulite-facies metabasite ejecta in the Laacher See area, Eifel, West Germany. *Lithos* **12**, 251–270.

Raikes, S. & Bonjer, K. P. (1983). Large-scale mantle heterogeneity beneath the Rhenish Massif and its vicinity from teleseismic P-residuals measurements. In: Fuchs, K., von Gehlen, K., Mälzer, H., Murawski, H. & Semmel, A. (eds) *Plateau Uplift*. Berlin: Springer, pp. 315–331.

Riley, T. R., Bailey, D. K., Harmer, R. E., Liebsch, H., Lloyd, F. E. & Palmer, M. R. (1999). Isotopic and geochemical investigation of a carbonatite–syenite–phonolite diatreme, West Eifel (Germany). *Mineralogical Magazine* **63**, 615–631.

Ritter, J. R. R., Jordan, M., Christensen, U. R. & Achauer, U. (2001). A mantle plume below the Eifel volcanic fields, Germany. *Earth and Planetary Science Letters* **186**, 7–14.

Rosenbaum, J. M. & Wilson, M. (1996). Two-stage enrichment of the Eifel mantle: new evidence. *Journal of Conference Abstracts* **1**, 523.

Rudnick, R. L. & Goldstein, S. L. (1990). The Pb isotopic compositions of lower crustal xenoliths and the evolution of lower crustal Pb. *Earth and Planetary Science Letters* **98**, 192–207.

Sachtleben, T. & Seck, H. A. (1981). Chemical control of Al-solubility in orthopyroxene and its implications on pyroxene geothermometry. *Contributions to Mineralogy and Petrology* **78**, 157–165.

Sisson, T. W. (1994). Hornblende–melt trace-element partitioning measured by ion microprobe. *Chemical Geology* **117**, 331–344.

Stein, M. & Hofmann, A. W. (1992). Fossil plume head beneath the Arabian lithosphere? *Earth and Planetary Science Letters* **114**, 193–209.

Stosch, H. G. (1987). Constitution and evolution of subcontinental upper mantle and lower crust in areas of young volcanism: differences and similarities between Eifel (F. R. Germany) and Tariat Depression (central Mongolia) as evidenced by peridotite and granulite xenoliths. *Fortschritte der Mineralogie* **65**, 49–86.

Stosch, H. G. & Lugmair, G. W. (1986). Trace element and Sr and Nd isotope geochemistry of peridotite xenoliths from the Eifel (West Germany) and their bearing on the evolution of the subcontinental lithosphere. *Earth and Planetary Science Letters* **80**, 281–298.

Stosch, H. G. & Seck, H. A. (1980). Geochemistry and mineralogy of two spinel peridotite suites from Dreiser Weiher, West Germany. *Geochimica et Cosmochimica Acta* **44**, 457–470.

Stosch, H. G., Carlson, R. W. & Lugmair, G. W. (1980). Episodic mantle differentiation: Nd and Sr isotopic evidence. *Earth and Planetary Science Letters* **41**, 263–271.

Stosch, H. G., Lugmair, G. W. & Seck, H. A. (1986). Geochemistry of granulite facies lower crustal xenoliths: implications for the geological history of the lower continental crust underneath the Eifel/W. Germany. In: Dawson, B. J., Carswell, D. A., Hall, J. & Wedepohl, K. H. (eds) *The Nature of the Lower Continental Crust. Geological Society, London, Special Publications* **24**, 309–317.

Stosch, H. G., Schmucker, A. & Reys, C. (1992). The nature and geological history of the deep crust under the Eifel, Germany. *Terra Nova* **4**, 53–62.

Sweeney, R. J., Green, D. H. & Sie, S. H. (1992). Trace and minor element partitioning between garnet and amphibole and carbonatitic melt. *Earth and Planetary Science Letters* **113**, 1–14.

Sweeney, R. J., Prozesky, V. & Przybylowicz, W. (1995). Selected trace and minor element partitioning between peridotite minerals and carbonatite melts at 18–46 kb pressure. *Geochimica et Cosmochimica Acta* **59**, 3671–3683.

Wedepohl, K. H. & Baumann, A. (1999). Central European Cenozoic plume volcanism with OIB characteristics and indications of a lower mantle source. *Contributions to Mineralogy and Petrology* **136**, 225–239.

Wedepohl, K. H., Gohn, E. & Hartmann, G. (1994). Cenozoic alkali basaltic magmas of western Germany and their products of differentiation. *Contributions to Mineralogy and Petrology* **115**, 253–278.

Wilson, M. (1996). HIMU mantle plumes, hot lines and hot blobs: Sr–Nd–Pb isotopic constraints for the Mesozoic–Cenozoic evolution of their mantle sources. *Journal of Conference Abstracts* **1**, 675.

Wilson, M. & Downes, H. (1991). Tertiary–Quaternary extension-related alkaline magmatism in Western and Central Europe. *Journal of Petrology* **32**, 811–849.

Wilson, M. & Patterson, R. (2001). Intraplate magmatism related to short-wavelength convective instabilities in the upper mantle: evidence from Tertiary–Quaternary volcanic province of western and central Europe. *Geological Society of America, Special Papers* **352**, 37–58.

Witt, G. & Seck, H. A. (1989). Origin of amphibole in recrystallized and porphyroclastic mantle xenoliths from the Rhenish Massif: implications for the nature of mantle metasomatism. *Earth and Planetary Science Letters* **91**, 327–340.

Witt-Eickschen, G. & Harte, B. (1994). Distribution of trace elements between amphibole and clinopyroxene from mantle peridotites of the Eifel (western Germany): an ion-microprobe study. *Chemical Geology* **117**, 235–250.

Witt-Eickschen, G. & Kramm, U. (1998a). Mantle upwelling and metasomatism beneath central Europe: geochemical and isotopic constraints from mantle xenoliths from the Rhön (Germany). *Journal of Petrology* **38**, 479–493.

Witt-Eickschen, G. & Kramm, U. (1998b). Evidence for the multiple stage evolution of the subcontinental lithospheric mantle beneath the Eifel (Germany) from pyroxenite and composite pyroxenite/peridotite xenoliths. *Contributions to Mineralogy and Petrology* **131**, 258–272.

Witt-Eickschen, G., Seck, H. A. & Reys, C. (1993). Multiple enrichment processes and their relationships in the subcrustal lithosphere beneath the Eifel (Germany). *Journal of Petrology* **34**, 1–22.

Witt-Eickschen, G., Kaminsky, W., Kramm, U. & Harte, B. (1998). The nature of young vein metasomatism in the lithosphere of the West Eifel (Germany): geochemical and isotopic constraints from composite mantle xenoliths from the Meerfelder Maar. *Journal of Petrology* **39**, 155–185.

Witt-Eickschen, G., Klemd, R. & Seck, H. A. (2003). Density contrast of melt (glass) associated fluid inclusions from two distinct suites of mantle peridotites from the West Eifel, Germany: implications for melt origin. *Contributions to Mineralogy and Petrology* (in press).

Woolley, A. R. & Kempe, D. R. C. (1989). Carbonatites: nomenclature, average chemical compositions, and element distribution. In: Bell, K. (ed.) *Carbonatites: Genesis and Evolution*. London: Unwin Hyman, pp. 1–14.

Wörner, G., Zindler, A., Staudigel, H. & Schmincke, H. U. (1986). Sr, Nd, and Pb isotope geochemistry of Tertiary and Quaternary alkaline volcanics from West Germany. *Earth and Planetary Science Letters* **79**, 107–119.

Yaxley, G. M., Green, D. H. & Kamenetsky, V. (1998). Carbonatite metasomatism in the southeastern Australian lithosphere. *Journal of Petrology* **39**, 1917–1930.

Zindler, A. & Hart, S. R. (1986). Chemical geodynamics. *Annual Review of Earth and Planetary Sciences* **14**, 493–571.